

ScholarWorks@GSU

Delineating Optimal Solar Sites in Atlanta Using GIS and Remote Sensing

Authors	Appiah, Sam Yaw
Citation	Appiah, Sam Yaw. Delineating Optimal Solar Sites in Atlanta Using GIS and Remote Sensing. Dec. 2021, Georgia State University. https://doi.org/10.57709/26842090 .
DOI	https://doi.org/10.57709/26842090
Download date	2026-05-13 15:53:51
Link to Item	https://hdl.handle.net/20.500.14694/6360

Delineating Optimal Solar Sites in Atlanta Using GIS and Remote Sensing

by

Sam Appiah

Under the Direction of Lawrence Kiage, PhD

A Thesis Submitted in Partial Fulfillment of the Requirements for the Degree of

Master of Science

in the College of Arts and Sciences

Georgia State University

2021

ABSTRACT

Increasing global energy demand presents the challenge of insufficient supply of energy in cities and an ever-increasing carbon footprint. Out of the plethora of renewable energy options, solar energy presents the most viable option as it is geographically unconstrained. Implementation of a solar project requires solar resource assessment and consideration of limiting factors such as slope aspect, temperature and GHI. Multi-criteria selection method is often used in delineating optimal site for the establishment of solar farms. The purpose of this study was to determine solar index of optimal site selection for solar farms by using satellite images, GIS and AHP in the study area. The final composite index yielded the three categorizations of least suitable, moderately suitable, and most suitable areas. The resulting size and percentage of the study area optimal for solar panels was 3% and 234.96 sq km respectively.

INDEX WORDS: Solar Resource Assessment, Heliosat, AHP, GIS, Remote Sensing

Copyright by
Sam Appiah
2021

Delineating Optimal Solar Sites in Atlanta Using GIS and Remote Sensing

by

Sam Appiah

Committee Chair: Lawrence Kiage

Committee: Ricardo Nogueira

Dajun Dai

Electronic Version Approved:

Office of Graduate Services

College of Arts and Sciences

Georgia State University

December 2021

DEDICATION

This thesis is dedicated to my father, Sam Asare Baffour, whose unflinching support and insightful counsel has been the bedrock for my accomplishments to date.

ACKNOWLEDGEMENTS

I would like to express my sincere gratitude to Dr Lawrence Kiage for his patience, understanding and immense contribution towards the fruition of this thesis. A heartfelt appreciation goes out to the members of my committee Dr Dajun Dai and Dr Ricardo Nogueira, for their counsel and contribution to my thesis. A special thank you goes out to my sister, Elizabeth Sam, for her words of encouragement and unyielding support.

Lastly, I would like to thank my family, without whose support I would not be who I am today.

TABLE OF CONTENTS

ACKNOWLEDGEMENTS		V
LIST OF TABLES		VIII
LIST OF FIGURES		IX
LIST OF ABBREVIATIONS		XI
1 INTRODUCTION		1
2 LITERATURE REVIEW		3
2.1 Ground-Based And Satellite-Based Solar Irradiance Data		3
2.2 Satellite-Based Estimates of Solar Potential		3
<i>2.2.1 Theoretical Framework of Satellite Estimation</i>		<i>4</i>
<i>2.2.2 Estimation of SSI From Satellites</i>		<i>5</i>
2.3 Selection of Optimal Sites Using Geographical Information Systems (GIS)		7
2.4 Research Problem		8
2.5 Research Objective		9
3 METHODOLOGY		10
3.1 Study Area		10
3.2 Data		11
3.3 Heliosat-2 Methodology		12
<i>3.3.1 Calculating Global Horizontal Irradiance</i>		<i>13</i>
<i>3.3.2 Cloudless Surface Solar Irradiance (SSI)</i>		<i>13</i>

3.3.3	<i>Beam Component</i>	13
3.3.4	<i>Diffuse Component</i>	14
3.3.5	<i>Calculation of GHI Under Overcast Conditions</i>	15
3.4	Comparison of Calculated GHI With Ground Measured GHI	16
3.5	Site Selection and Multi-Criteria Decision Analysis	18
3.5.1	<i>Identifying Physical Suitability Criteria</i>	18
3.5.2	<i>Developing a Composite Suitability Index</i>	19
3.5.3	<i>Identifying Sites Suitable for Mounting Solar Panels</i>	22
4	RESULTS	23
4.1	Calculated Monthly and Annual GHI Values	23
4.2	Validation of The Heliosat-2 Methodology	24
4.3	Resulting Comparison Matrix and Weights of Physical Factors	26
4.4	Resulting Normalized Raster Surfaces	27
4.5	Solar Composite Index	32
5	DISCUSSION	34
6	CONCLUSION	38
7	RECOMMENDATION AND FUTURE WORK	39
	REFERENCES	40

LIST OF TABLES

Table 1 Attributes of the datasets used in this research study	12
Table 2 A table of the list of the identified physical suitability criteria/factors	19
Table 3 A table of the Likert Scale	22
Table 4 Results statistical parameters used for the comparison of the Heliosat-2 values and ground-based station values	25
Table 5 Weights of various favorable criteria indicators.....	27

LIST OF FIGURES

Figure 1 Simplified relations between satellite observations and SSI according to one-dimensional radiative transfer theory for a) clear sky and b) cloudy sky (Huang et al., 2020).	5
Figure 2 A map showing the geographical limits of the study area. It includes all the ten counties that makeup Metropolitan Atlanta	10
Figure 3 A graph showing the monthly GHI values for Metropolitan Atlanta. Atlanta received its highest solar radiation values during the months of May, June, and July	23
Figure 4 Annual GHI values for Metropolitan Atlanta. The values ranged between 3690 watts per meter squared to 4249 watts per meter squared.....	24
Figure 5 Results of the statistical parameters of MBE and RMSE used in the validation of calculated GHI compared against ground station measured value from the NREL network	26
Figure 6 Normalized aspect raster data indicating areas favorable for solar siting based on only the aspect criterion	28
Figure 7 A normalized slope map of Metropolitan Atlanta showing suitable areas for mounting solar panels based on the slope criterion alone	29
Figure 8 The map displays the normalized values of the annual GHI values of Atlanta. Blue indicates areas least favorable per the GHI criterion, while the red color shows the most area.....	30
Figure 9 Normalized temperature values for Metropolitan. Areas with values of 0.75 and above are not susceptible to decreased efficiency because of temperature.....	31

Figure 10 Normalized Map of Land Cover of Metropolitan Atlanta showing areas of bare ground designation. Developed areas unsuitable for solar siting are shown in the black coloration, while suitable areas are shown via the white coloration..... 32

Figure 11 A map showing the solar composite suitability index for Metropolitan Atlanta. 33

LIST OF ABBREVIATIONS

GHI – Global Horizontal Irradiance

SSI – Surface Solar Irradiance

AHP – Analytical Hierarchy Process

TOA – Top of The Atmosphere

BSRN – Baseline Surface Radiation Network

ARM – Atmospheric Radiation Measurement

RTM – Radiative Transfer Model

GIS – Geographic Information System

TOMS - Total Ozone Mapping Spectrometer

MODIS - Moderate Resolution Imaging Spectroradiometer

DEM – Digital Elevation Model

QGIS – Quantum Geographic Information System

NREL – National Renewable Energy Laboratory

CR – Consistency Ratio

RMSE – Root Mean Square Error

MBE – Mean Bias Error

MAE – Mean Absolute Error

PV- Photovoltaic

1 INTRODUCTION

Meeting the energy demands of the world is one of the most challenging needs that face humanity today (Jarvis et al, 2012; Gasparovic, 2019; Dazhi et al., 2015; Mierzwiak and Calka, 2017). Yet, in recent times, advancement in the technology needed to extract fossil fuels has led to increased production of energy, widespread accessibility to energy, and consequently massive consumption of energy (Jarvis et al., 2012). While the increased accessibility to energy worldwide is welcomed, the environmental toll caused by the accompanying consumption of fossil fuel cannot be ignored (Gasparovic, 2019). The negative consequence has shifted the world's focus towards developing sustainable energy sources (Schneider et al., 2000). Renewable energy sources such as solar power, wind power, hydropower, biomass, and geothermal energy present many options (Gasparovic, 2019). However, solar energy has emerged as one of the most promising alternatives.

Solar energy impinging on the surface of the Earth is widely distributed over the surface of the Earth in abundant quantities, thus fostering a concerted global effort in investing in them. This property of solar energy is of great advantage as the benefits of solar energy can be harnessed everywhere. Knowledge of local solar radiation is the key to implementing solar energy systems (Gasparovic, 2019). The viability of a solar energy project relies on the bankability of the amount of surface solar irradiance available at the chosen site. Solar energy resource assessment is determined by either measurement of radiation values from local ground stations or by satellite observations (Ohmura et al., 1998). However, the network of accurate ground-based solar measurement stations is sparse, and the interpolation of solar data from these stations is inadequate to satisfy the standards required for constructing a solar plant (Ohmura et al., 1998). In lieu of this, solar products from geostationary satellite images have become the industry standard for

preliminary assessment of solar potential in areas where ground-based measurement is lacking (Hafeznia et al., 2017).

2 LITERATURE REVIEW

2.1 Ground-Based And Satellite-Based Solar Irradiance Data

The exploitation of solar energy is dependent on the accurate quantification of the amount of solar radiation that impinges on the surface of the Earth under consideration (Huang et al., 2020). A review of current data repositories of solar resources classified the databases into two categories: satellite-derived databases and ground-based databases (Huang et al., 2020). The ground-based solar radiation database is derived from solar irradiance measurements made by radiometers. Gueymard (2009) identified the three primary sources of ground-based solar measurement as solar monitoring sites, conventional long-term measurements by weather monitoring stations, and research sites (Atmospheric Radiation Measurement (ARM) program or the Baseline Solar Radiation Network (BSRN)). Given the reliance on empirical and theoretical models of meteorological stations and research sites, data captured from these sources is measured by proven techniques with robust instruments that derive the highest accuracy possible (Geuder et al., 2006).

The HelioClim-3 databases (version 4 and version 5) and the Copernicus Atmosphere Monitoring Radiation Service (version 2) are two of the several satellite solar databases that have been constructed from images captured by the Meteosat series of satellites (Marchand,2018).

2.2 Satellite-Based Estimates of Solar Potential

Satellite imagery offers one of the best opportunities to assess the incoming amount of solar insolation that reaches the surface of the Earth. As the temporal and spatial coverage of geostationary satellites has improved, it has become accepted to use solar satellite estimates from regions where ground stations are sparse or non-existent (Alonso-Montesinos et al., 2015). In its initial development, studies were critical of the relevant uncertainties between satellite

measurements and ground stations. Uncertainties are attributable to the inability of the solar algorithms to properly characterize atmospheric aerosols or account for the significant temporal changes in cloud cover and transmissivity. However, recent studies have proven satellite errors are within the range of uncertainties associated with ground measurements (Journée, 2010).

2.2.1 Theoretical Framework of Satellite Estimation

Satellites record both surface reflectance at the top of the atmosphere (TOA) and the atmosphere. The framework of deriving solar surface irradiance (SSI) is determined by accounting for the attenuation of incident solar radiation by the composition of the atmosphere. In principle, the effect of atmospheric constituents is determined either directly or indirectly from TOA radiances captured by the satellite (Bhartia et al., 1996). Consequently, the TOA readings are used as a proxy to quantify the solar radiation that impinges on the surface of Earth.

Ozone, water vapor, and aerosols have the most influence on the depletion of solar radiation on a clear sky day. Different amounts of these constituents in the atmosphere yields varying SSI values. Atmospheric constituents are wavelength-dependent. Hence, a comparison of the absorption profile of solar radiation specific to portions of the electromagnetic wavelengths to the atmospheric window enables the estimation of the amounts of constituents (water vapor, aerosols, and ozone) present in the atmosphere (Liu, 2017). Complementary ozone products from Total Ozone Mapping Spectrometer (TOMS) Earth Probe and MODIS enable the estimation of ozone content and gauge its effect on solar attenuation. The most significant regulator of SSI is cloud cover. The constant evolution of the theoretical framework and algorithm to estimate SSI is premised on perfecting the accounting process for the radiative attenuation by clouds and aerosols (scattering and absorption by clouds and aerosols) in the atmosphere. Solar depletion attributable to clouds is obtained from TOA satellite observations or

by using cloud data derived from raw satellite data (Huang, 2020). Figure 1 illustrates a simplified version of the interaction of shortwave radiation (visible radiation) with the atmosphere and the surface of the Earth on a clear-sky day and a cloudy day.

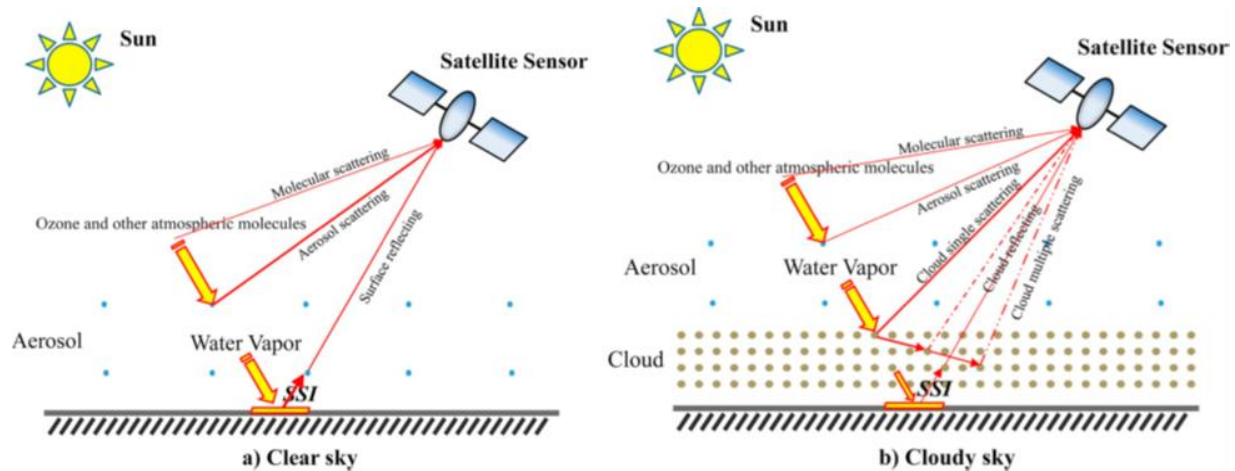


Figure 1 Simplified relations between satellite observations and SSI according to one-dimensional radiative transfer theory for a) clear sky and b) cloudy sky (Huang et al., 2020).

2.2.2 Estimation of SSI From Satellites

Several algorithms have been developed over the years to estimate surface irradiance values. These algorithms can be classified into two groups: RTM and Conventional Statistical Methods (Huang, 2020).

The Radiative Transfer Model (RTM) is based on the acquisition of atmospheric spectral properties and the development of radiative transfer equations to solve the problem of estimating accurate SSI. Popular RTM includes Moderate Resolution Atmospheric Transmission (MODTRAN) or LibRadtran (Emde, 2016; Mayer, 2020) used to calculate the surface solar insolation. The goal of radiative transfer models is to minimize spectral dependence, simplify radiative transfer solutions while maintaining the accuracy of methodologies that depend on them. However, it should be noted that it is costly to run RTMs, especially complex RTMs (Huang, 2020).

The conventional statistical method uses empirical-based functions to correlate satellite data to SSI values. The premise of the conventional statistical method is that the TOA reflectance measured by the satellite depends on the transmissivity of the cloud. The Heliosat Method, a popular conventional statistical method, uses an empirical model to calculate surface irradiances (Cano,1986; Rigollier, 2004). The empirical method uses the Linke turbidity factor to characterize the atmospheric transmittance. The Linke turbidity factor defines the effect of scattering and absorption by atmospheric gases and water vapor in the atmosphere.

The dynamic nature of atmospheric aerosols and the climatic nature of different geographic locations introduces biases that affect the efficacy and accuracy of the Heliosat model. Badescu et al., 2013 indicated the relevance of validating Heliosat models as it has never been validated in some regions with differences in atmospheric constituents compared to the area where the model was developed. Engerer et al., 2015 validated the statistical method in Australia using reference 1-min data from 14 sites and concluded the model produced differing accuracy levels in different climate zones of Australia. Dazhi et al., 2015 compared test the statistical models in Singapore, whose climate is generally equatorial and fully humid and concluded that the accuracy level of the model was not acceptable. Different statistical model validation studies were reviewed, and the performances of the models were found to be influenced by the aerosol profile of the region. Perez (1997) found the usage of surface measurements to calibrate or tune statistical methods substantially improved the accuracy of its solar estimates. Statistical method are commercially pervasive and are the default tool for solar energy assessment applications. A review of existing literature indicated no validation study of statistical method (Heliosat) had been conducted in an urban area such as Metropolitan Atlanta and an even limited work of validation of the model in the humid subtropic climatic zone of Atlanta.

2.3 Selection of Optimal Sites Using Geographical Information Systems (GIS)

Once the global horizontal irradiance(GHI) has been estimated for a region, it is imperative to refine parameters to determine active solar radiation at a small spatial resolution. Studies using GIS to analyze solar power plant siting have identified key determinants that affect the selection of an optimal site (Gasparovic,2019). It is critical to assess parameters (assigning weights) that contribute to the determination of sites to leverage the full potential of solar radiation. The work of Gasparovic (2019) identified these physical parameters such as slope, aspect, temperature, sunshine duration, and land-use restrictions

Slope and aspect (constraint factors) affect the intensity of solar radiation that the solar panels can harness. Studies have shown that panels oriented southward coupled with a sloping incline of less than 10% generate the highest quantity of electricity (Mierzwiak and Calka, 2017). Thus, the factors of slope and aspect are unproductive as they restrict the availability of probable optimal solar farm sites. Likewise, temperature as a variable is negative (constraining factor) as the study of Mierzwiak and Calka, 2017, Mujabar, 2021 correlated drop in electricity production to increased temperature. However, sunshine hours and GHI were favorable factors as increasing values of these criteria correlate with increased electricity generation from the solar panel systems (Mierzwiak and Calka, 2017). The exploitation of local solar resources is constrained by space and local physical conditions/ecosystems. Essentially, all solar project development is local, and specific knowledge of the locale is essential for a rewarding project development process. For the development of PV farms in Metropolitan Atlanta, suitability analysis is an indispensable process conducted via GIS.

2.4 Research Problem

At the 2015 United Nations Climate Change conference, Atlanta resolved to reduce the city's greenhouse gas and carbon dioxide emissions by exploiting renewable energy alternatives (Clean Energy Atlanta, 2017). Following the conference, Atlanta's city council passed a resolution on May 1, 2017, requiring the mayor's office to develop a plan for the city to achieve 100% clean energy by 2035 (Clean Energy Atlanta, 2017). The resolution called for the exploitation and development of renewable energy as the preferred option. The city is adopting solar energy to achieve its 100% clean energy aspiration. Programs such as Solar Atlanta is adding 1.3 MW to 24 municipal buildings via solar panels (Clean Energy Atlanta, 2017).

Presently, solar energy accounts for only 6% of Atlanta's energy portfolio, and the city plans to construct large solar farms to meet half of the city's energy demand. Mega-scale solar farms in Atlanta would require accurate solar radiation data from satellite estimates.

The geographic confine of Metropolitan Atlanta lacks the density or network of ground solar stations needed to interpolate accurate solar data for the city. Thus, satellite estimates of global horizontal irradiation impinging on Atlanta will be calculated by conventional statistical methods (Heliosat-2). This presents an interesting challenge as the Heliosat-2 method has never been validated in an urban setting, nor has the accuracy method been assessed in a humid sub-tropic climatic zone solar. It is essential to assess the accuracy of the estimations using solar data derived from the ground data.

Subsequently, once solar data is derived, identifying suitable solar farm sites requires the consideration of local characteristics and the numerous parameters that affects the processes for modeling the exact amount of solar insolation received by points of interest. Metropolitan has an

unparallel ecosystem of characteristics and parameters whose exact effect on incident solar radiation will need to be considered when determining areas suitable for solar farms.

This thesis is an attempt to satisfy these requirements by answering the following questions:

- How does the accuracy of Atlanta's GHI estimates derived from the Heliosat-2 method compare to that of ground measured solar radiation data?
- What is the size of the optimal sites available in Metropolitan Atlanta for mounting solar panels when the effect of physical environmental factors are considered?

2.5 Research Objective

A review of existing literature reveals studies involving solar resource assessment falls into two classes. The first class entails studies that are purposely conducted to validate solar data estimated from statistical models, and the second class comprise studies that uses already validated solar data and physical variables to delineate solar site. This study is a merger of both classes of studies.

- 1) The first objective of this research study was to use satellite data to calculate GHI incidents in Metropolitan Atlanta and validate the calculated GHI against values measured by ground stations
- 2) The second objective of this research study was to identify the optimal sites for mounting solar panels in Metropolitan Atlanta using physical factors that affect incident solar GHI

3 METHODOLOGY

3.1 Study Area

The chosen study area for this research is Metropolitan Atlanta. Metropolitan Atlanta is located on 33°45'18"N latitude, 84° 23' 16.737" W longitude and has a sub-tropical climate. Metropolitan Atlanta has a population of 6,089,815 per the recent 2020 census and has an average population density of 1,416.78 km sq. Metropolitan Atlanta comprises ten counties: Fulton, DeKalb, Gwinnett, Cobb, Clayton, Rockdale, Cherokee, Fayette, Douglas, and Henry. The metropolitan Atlanta area occupies a land size of 7832.124 km sq. The extent of the geographic area of the study is shown in Figure 1 below.

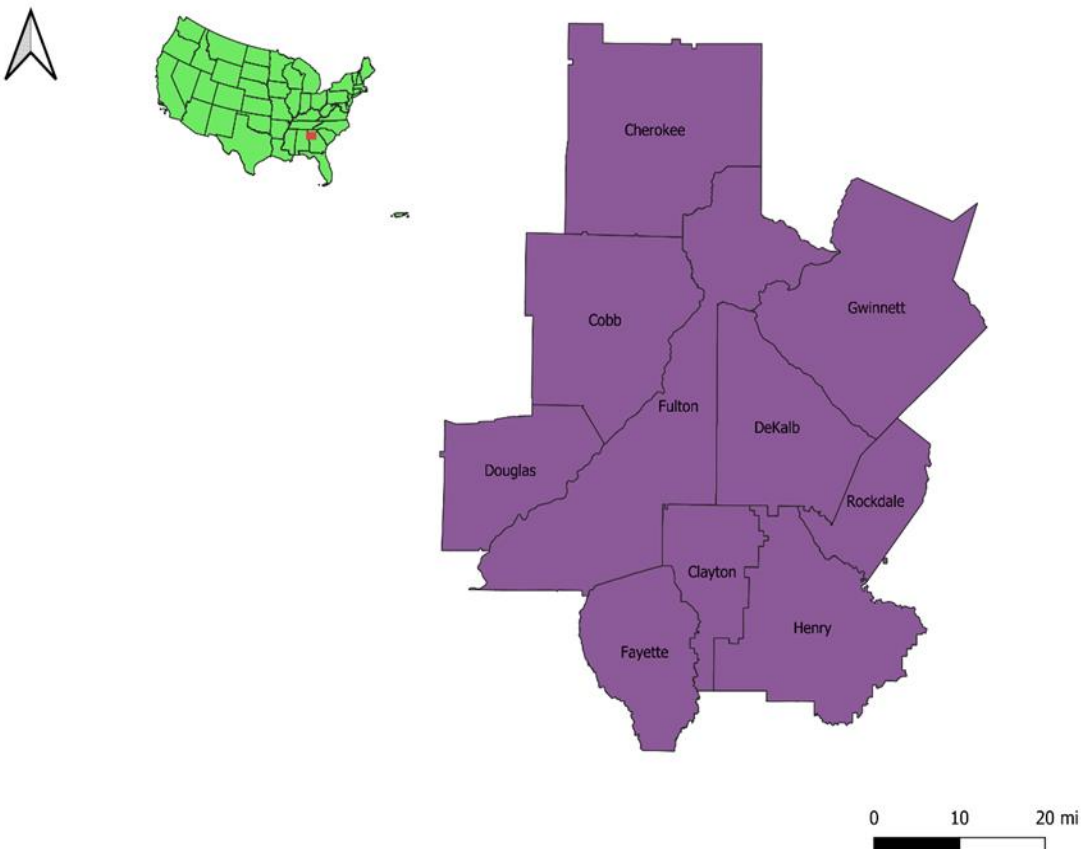


Figure 2 A map showing the geographical limits of the study area. It includes all the ten counties that makeup Metropolitan Atlanta

3.2 Data

The methodology adopted was implemented in two stages. The first stage involved the calculation of global horizontal irradiation using Linke Turbidity and clearness index as input parameters (Table 1). While the second stage distinguished favorable sites using multi-criteria selection factors such as slope, aspect temperature, land cover, global horizontal irradiance, and sunshine hours. Each stage of the methodology of this research project required different raster datasets.

Raster datasets of Linke turbidity, clearness index, Digital Elevation Model (DEM), temperature, hours of sunshine, and land cover types for metropolitan Atlanta were downloaded. Linke turbidity data were downloaded from the SoDa solar radiation project. The SoDa project is a European Union initiative tasked with monitoring the energy exchange between the surface of the Earth and the atmosphere. As a result, the project continually produces monthly averages of Linke turbidity data at a spatial resolution of 1 km. Clearness index data for metropolitan Atlanta were downloaded from the HOMER Pro project, which compiles monthly clearness index values for geographic locations worldwide.

The physical factors of annual average hours of sunshine, aspect, and slope were calculated using `r.sun`, `r.aspect`, and `r.slope` geoprocessing tools of QGIS. `r.slope` and `r.slope` are geoprocessing tools that generate a raster map of slope and aspect from an input of a raster DEM. Similar to `r.aspect` and `r.slope`, the `r.sun` is also a QGIS geoprocessing tool that produces a raster map indicating the average annual hours of sunshine hours given a specific geographic location (point) or an area (polygon). DEM and annual surface temperatures were downloaded from Diva GIS and climate signals, respectively. Finally, the 2019 land cover classification of

the study area was downloaded from the Multi-Resolution Land Characteristics consortium group's land cover classification dataset database.

Table 1 shows a detailed description of the datasets that were used in this research study

Table 1 Attributes of the datasets used in this research study

Data	Data Production Date	Resolution	Source	Data Type
Metropolitan Atlanta Boundary Linke Turbidity	2019	N/A	Atlanta Regional Commission(atlantaregional.org)	Feature Class
Clearness Index	2019	N/A	Homer Pro(www.homerenergy.com/products/pro/docs/latest/clearness_index.html)	Raster
Sunshine Hours	2019	10m	r.sun(QGIS tool)	Raster
Aspect	2019	10m	r.aspect(QGIS tool)	Raster
Slope	2019	10m	r.slope(QGIS tool)	Raster
Land Cover	2019	10m	Multi-Resolution Land Characteristics (MRLC) (mrlc.gov)	Raster
Temperature	2019	3m		Raster
Global Horizontal Irradiance (GHI)	2019	N/A	National Renewable Energy Laboratory(nrel.gov)	Point Feature
Digital Elevation Model	2019		Diva GIS(diva-gis.org)	Raster

3.3 Heliosat-2 Methodology

The Heliosat-2 method maintains the core principles of cloud index and clear-sky irradiance from Heliosat-1. However, satellite inputs into Heliosat-2 are radiances rather than the numerical counts in Heliosat (Rigollier, 2004). The change allows for the calculation of gain and calibration for long-term measurements. Also, it factors into account the effect of change of sensors. Fundamentally, the Heliosat-2 method shifts the over-reliance of the previous method on empirical parameters to the usage of known physical parameters.

3.3.1 *Calculating Global Horizontal Irradiance*

In calculating the annual solar insolation that impinged on the surface of our study area, the r.sun geoprocessing tool of QGIS was used. The r.sun model is based on the Heliosat-2 methodology developed by the European Solar Radiation Atlas project.

3.3.2 *Cloudless Surface Solar Irradiance (SSI)*

The Heliosat-2 model first calculates global horizontal irradiation by calculating the cloudless surface solar insolation. On a cloudless day, the SSI reaching the surface is a combination of the direct beam component and the diffused fraction of the incident extra-terrestrial solar radiation that permeates the Earth's atmosphere to reach the surface of the earth. The beam component is the portion of the extra-terrestrial irradiance that travels directly from the top of the atmosphere to the Earth's surface without experiencing any reflection or refraction, while the diffused fraction quantifies the irradiance reflected by the gases and aerosols present in the atmosphere. Equation 1 below demonstrates how the clear-sky global horizontal irradiance was calculated for this study.

$$G_{clear-sky} = B + D \quad \text{eq. (1)}$$

Where $G_{clear-sky}$ is SSI under cloudless conditions, B is beam irradiance, and D is the diffused irradiance.

3.3.3 *Beam Component*

The beam component of the incoming solar radiation was calculated by quantifying the amount of solar radiation impinging on the surface under the condition of a clear sky. A clear sky condition refers to a state where the atmosphere was cloudless; thus, the incident surface beam solar radiation was accounted for by subtracting the lost solar radiation attributable to Rayleigh scattering, scattering by aerosols and the absorption of radiation by the gaseous composition from

the incident extra-terrestrial irradiance. The formula used for the calculation of the beam component is shown in equation 2:

$$B = G_0 \exp \{-0.8662 T_{LK} M \partial_R(m)\} \quad \text{eq. (2)}$$

G_0 is the extra-terrestrial irradiance incident upon the top of the atmosphere, and the term $-0.8662 T_{LK}$ is the Linke atmospheric turbidity factor (Linke turbidity is dimensionless) corrected by Kasten (1996) for an air mass of two. The parameter M in equation (1) is the relative optical air mass and ∂_R is Rayleigh optical thickness of the atmosphere.

3.3.4 Diffuse Component

Under cloudless conditions, as the atmosphere becomes more turbid, the diffuse irradiance increases while the beam irradiance decreases. The estimation of the diffuse component on a horizontal surface $D [Wm^{-2}]$ is made as a product of the normal extraterrestrial irradiance G_0 , a diffuse transmission function T_n dependent only on the Linke turbidity factor T_{LK} and a diffuse solar altitude function F_D dependent only on the solar altitude h_0 (Scharmer and Greif 2000):

$$D = G_0 T_n(T_{LK}) F_D(h_0) \quad \text{eq. (3)}$$

The r.sun geoprocessing tool accepts as input a raster dataset of the Linke turbidity of the area for which the cloudless SSI is being calculated. The monthly averages of Linke turbidity of the study area were inputted as a parameter of the r.sun geoprocessing tool designated for Linke turbidity, and the cloudless SSI was calculated for each month of the year 2019.

3.3.5 Calculation of GHI Under Overcast Conditions

The typical normal weather condition has no cloudless days (NREL, 2021). Metropolitan Atlanta has 217 mostly sunny days annually (NREL, 2021). Yet even on the mostly sunny days, 25% of the sky was covered in clouds during the daylight hours (NREL, 2021).

Cloud cover has a significant impact on solar radiation reaching the surface. Thus, to truly quantify the GHI impinging on the surface of the study area, the overcast irradiance was calculated from the clear-sky GHI raster data calculated from equation (1) via a factor that parameterizes the attenuation of incoming solar radiation by clouds. This factor is known as the clearness index. The clearness index (K_c) represents the atmospheric transmission of clouds expressed as a ratio between the global radiation under overcast and clear-sky conditions. The clearness index accounts for the different states of cloud cover (Rigollier, 2004). The clearness index is dimensionless and varies between 0 to 1. 1 indicates 100% transmissivity while 0 correlates to no transmissivity. At any point, the percentage of incident extra-terrestrial solar radiation reaching the surface of Earth is dependent on the transmissivity of the cloud. The Heliosat-2 method calculated the SSI on any day using the equation 4:

$$G = G_{clear-sky}K_c \quad (4)$$

Where G is the global horizontal irradiance under normal weather conditions, $G_{clear-sky}$ is the global horizontal irradiance on a cloudless day and K_c is the clearness index representing the transmissivity of the clouds present in the atmosphere at any point in time.

3.4 Comparison of Calculated GHI With Ground Measured GHI

It is the standard practice to compare calculated GHI values from the Heliosat-2 methodology to GHI values measured by ground stations. To analyze the GHI values resulting from the implemented Heliosat-2 method, a validation against measurements made by ground stations was done. Firstly, the selected solar values calculated from the Heliosat-2 methodology corresponding to the locations of the control ground stations were extrapolated from the calculated GHI raster dataset. Secondly, measurements recorded during 2019 at the network of ground stations belonging to the National Renewable Energy Laboratory (NREL) were obtained

The NREL is a government science initiative that seeks to advance the sciences and engineering of energy efficiency, sustainable transportation, and renewable power technologies and provides the knowledge to integrate and optimize energy systems. The NREL has a network of partner ground stations that measure ground solar radiation and outputs average annual solar radiation values as part of this mission.

Some statistical parameters were calculated to compare the results provided by the Heliosat-2 methodology and the measured ground station values for the research study. These parameters are:

- Mean Absolute Error (MAE):

The mean absolute error is a statistical parameter that measures the errors between paired observations expressing the same phenomenon.

$$MAE = \frac{1}{n} \sum_{i=1}^n |p_i - m_i| \quad \text{eq. (5)}$$

Where p_i is the estimated values, m_i is the measured values, and n represents the number of compared values.

- MAE (%): Mean Absolute Error (%):

The mean absolute percentage error (MAPE) is the mean or average of the absolute percentage errors of forecasts. Error is defined as actual or observed value minus the forecasted value. The mean absolute percentage error for the calculated GHI of our study area and its accompanying measured GHI from the same area was calculated using equation 6 below

$$MAE(\%) = 100 \frac{MAE}{\bar{m}} \quad \text{eq. (6)}$$

where \bar{m} is the mean of the measured values.

- MBE: Mean Bias Error:

MBE quantified the overall bias and detected if the Heliosat-2 model is producing overestimation (MBE>0) or underestimation (MBE<0). The mean bias error for the calculated GHI and the measured GHI was derived using equation 7 below:

$$MBE = \frac{1}{n} \sum_{i=1}^n (p_i - m_i) \quad \text{eq. (7)}$$

Where p_i is the estimated values, m_i is the measured values, and n represents the number of compared values.

- MBE (%): Mean Bias Error (%):

The mean bias error for this research measured the average of percentage biases between the calculated GHI from the Heliosat-2 using the equation 8 below

$$MBE(\%) = 100 \frac{MBE}{\bar{m}} \quad \text{eq. (8)}$$

where \bar{m} is the mean of the measured values.

- RMSE: Root Mean Square Error:

The RMSE is the square root of the average of the squared differences between forecast and observed values. The value of the RMSE can be interpreted as the average error one can expect. The RMSE calculated during this study was to measure the accuracy of the calculated GHI from the methodology.

$$RMSE = \sqrt{\frac{1}{n} \sum_{i=1}^n (p_i - m_i)^2} \quad \text{eq. (9)}$$

p_i is the estimated values, m_i is the measured values, and n represents the number of compared values.

- RMSE (%): Root Mean Square Error (%):

$$RMSE(\%) = 100 \frac{RMSE}{\bar{m}} \quad \text{eq. (10)}$$

3.5 Site Selection and Multi-Criteria Decision Analysis

In identifying the sites in Metropolitan Atlanta that would be favorable to building solar farms, the multi-criteria decision analysis was adopted. The methodology consisted of identifying the physical suitability factors, developing a composite site suitability index and delineating a suitable site.

3.5.1 Identifying Physical Suitability Criteria

This step involved the identification of a list of criteria and the analysis of criteria primarily. The identified physical suitability criteria are listed below:

- Global Horizontal Irradiance (Solar Radiation): The selected sites for solar farms should receive relatively high solar radiation.
- Physical Suitability: The physical suitability factors refer to a list of conditions that affect the performance of solar power systems. These factors include climatic variables such as temperature, sunshine duration and topographic variables, particularly slope and aspect.
- Land Availability: The selected site for the solar farm should be bare or empty spaces that are currently not being used for any activity.

The listed criteria above were then put into two categories of Boolean and favorable factors.

Land availability was categorized as Boolean and reclassified into the binary of 0 and 1. 0

represented areas that were classified as developed, forest, water bodies and essentially any space that was not barren. 1 was assigned to areas that had a land cover class of either bare or barren. The other physical factors such as GHI, sunshine hours, aspect and slope were put in the category of favorable. The table 2 below shows the list of identified criteria as either favorable or Boolean:

Table 2 A table of the list of the identified physical suitability criteria/factors

Criteria	Type	Indicator	Unit	Relationship
Solar Irradiation	Favorable	GHI	W/m^2	Positive
Physical	Favorable	Sunshine Hours	Hour	Positive
Suitability				
		Aspect	°	Negative
		Slope	°	Negative
		Temperature	°C	Negative
Land Availability	Boolean	Bare/Barren		Logical

3.5.2 Developing a Composite Suitability Index

Composite indices are usually used in supporting the decision-making process through summarizing multi-dimensional realities and reducing the visible size of a set of indicators without disregarding the underlying information base (OECD). For this study, a composite suitability index was created by factoring in all the indicators listed in Table 2.

The indicators listed as favorable were normalized by one of the two listed formulae below:

$$N_x = \frac{X - X_{min}}{X_{max} - X_{min}} \quad \text{eq. (10)}$$

$$N_x = 1 - \left[\frac{X - X_{min}}{X_{max} - X_{min}} \right] \quad \text{eq. (11)}$$

Where:

N_x = normalized pixel value

X = Pixel value

X_{min} = minimum pixel value in the raster surface

X_{max} = maximum pixel value in the raster surface

The usage of the two formulae above ensured the range values for the normalized indicator/criteria fell within 0 to 1, with 0 representing the least suitability while 1 represented the highest suitability.

All the indicators/criteria which had a positive relationship were deemed as increasing the efficiency of solar systems were normalized using equation 10. GHI and sunshine duration raster were normalized using equation 10, while the raster surfaces of temperature and slope were normalized using equation 11 because of their negative effects on the efficiency of a solar system.

The normalization of the aspect raster surface was undertaken in two steps. Firstly, the aspect raster surface was reclassified into five classes according to the Likert scale (1– 9) shown in Table 3. The pixels with southward orientation were assigned a value of 9, and pixels with northward orientation were assigned a value of 1. Next, the generated binary raster surface was normalized according to equation 11.

Weights to the individual factors influencing the siting of the solar system were assigned using the Analytical Hierarchy Process (AHP). AHP allows for the designation of relative weights for different factors through applying pairwise comparisons (Whitaker, 2007).

According to pairwise comparisons (Hassan,2020), the relative importance of all considered indicators was compared and evaluated to each other according to an evaluation scale ranging from 1 to 9. Stemming from the pairwise comparison; a reciprocal matrix was produced, where each element in the matrix represents the dominance of a particular factor over the another in terms of their suitability for the siting of a solar farm. This was followed by dividing each element in the reciprocal matrix by the sum of its column. Finally, the weight of each factor was estimated by averaging across the rows (Khemiri et al., 2018; Uyan, 2013; Whitaker, 2007). Thereafter, the consistency of the estimated weights was assessed by calculating the Consistency Ratio (CR) (Khemiri et al., 2018) according to the following formula:

$$C.R = \frac{\lambda_{max} - n}{(n-1)*RI} \quad \text{eq. (12)}$$

where:

$C.R$ = Consistency ratio

λ_{max} = Maximum eigenvalue of the reciprocal matrix

n = Number of indicators

RI = Random consistency value = 1.12 in case of 5 indicators

Table 3 A table of the Likert Scale

Numerical value of P_{ij}	Definition
1	Equal importance of i and j
3	Moderate importance of i over j
5	Strong importance of i over j
7	Very strong importance of i over j
9	Extreme importance of i over j
2,4,6,8	Intermediate values

3.5.3 Identifying Sites Suitable for Mounting Solar Panels

Delineating the solar site involved calculating the composite suitability index by aggregating normalized raster surfaces of various favorable indicators based on their weights and multiplying the resulting aggregated raster surface by the binary land cover raster surface of the Boolean indicator according to the following equation 13:

$$S = x * \sum_{i=1}^n (N_i * W_i) \quad \text{eq. (13)}$$

Where:

S = Suitability index

x = Pixel value of binary raster surface representing Boolean criteria

N_i = Normalized pixel value of indicator I

W_i = Weight of indicator N_i

4 RESULTS

4.1 Calculated Monthly and Annual GHI Values

The results of the monthly GHI (Figure 3) values indicated January and December as having the lowest values of SSI throughout the year. As the data from figure 3 indicate, GHI gradually increased in value from January, with peak values recorded during the summer months of May, June, and July when GHI values of 5405.04 W/m^2 , 5430.7 W/m^2 , and 5321 W/m^2 were observed, respectively.

The annual GHI values (Figure 3) show the values of solar insolation impinging on Metropolitan Atlanta ranging from 3690 W/m^2 to 4249 W/m^2 . Figure 4 shows portions of Metropolitan Atlanta that recorded the highest value of incident GHI.

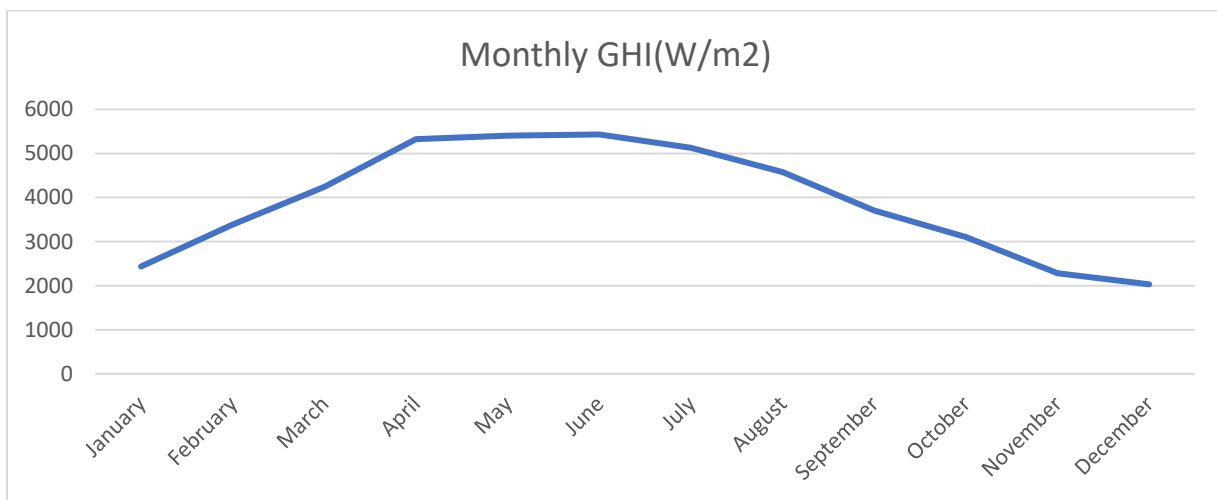


Figure 3 A graph showing the monthly GHI values for Metropolitan Atlanta. Atlanta received its highest solar radiation values during the months of May, June, and July

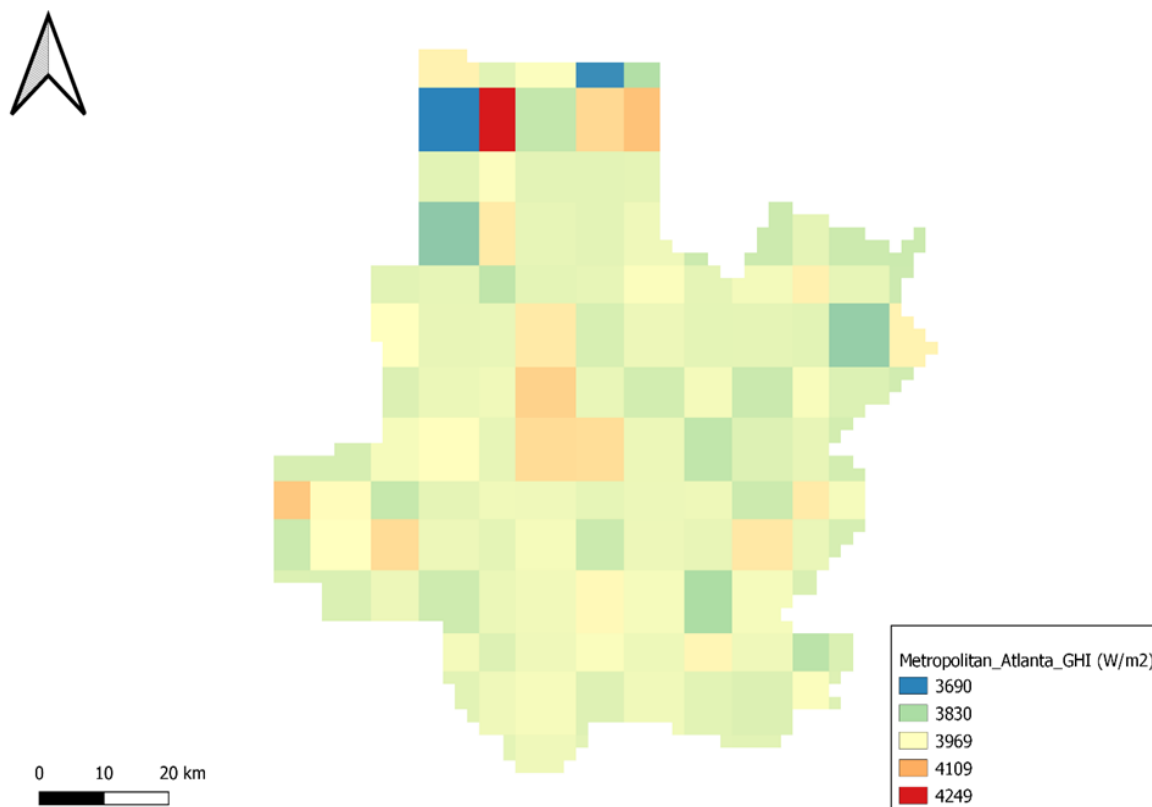


Figure 4 Annual GHI values for Metropolitan Atlanta. The values ranged between 3690 watts per meter squared to 4249 watts per meter squared

4.2 Validation of The Heliosat-2 Methodology

The statistical parameters used to validate the calculated Heliosat-2 GHI values revealed that the calculated GHI has a mean bias error of $-684.1 W/m^2$, the mean absolute error of $684.1 W/m^2$ And a root mean square error of $686.6345 W/m^2$.

The resulting values of MAE, RMSE, and MBE indicate an error of magnitude $684.1 W/m^2$ exists between the estimated value and the ground measured value. Overall, the Heliosat-2 method underestimates the recorded GHI value by 14%. The accuracy statistics of the calculated values have been summarized in Table 4 and visualized in figure 5.

Table 4 Results statistical parameters used for the comparison of the Heliosat-2 values and ground-based station values

COUNTY	Calculated	Observed	MAE	MAE(%)	MBE	MBE(%)	RMSE	RM
	GHI	GHI						
Fayette	3943.44678	4666.59	723.14322	14.78577	-	-14.7858	522936.1	14
							723.143	
Rockdale	4009.19189	4697.25	688.05811		-		473424	
							688.058	
Cobb	3911.13916	4550.02	638.88084		-		408168.7	
							638.881	
Clayton	3939.55615	4612.64	673.08385		-		453041.9	
							673.084	
Henry	3921.65625	4691.67	770.01375		-		592921.2	
							770.014	
Gwinnet	3950.73364	4601.88	651.14636		-		423991.6	
							651.146	
Fulton	3970.72266	4610.09	639.36734		-		408790.6	
							639.367	
Douglas	3902.95093	4565.82	662.86907		-		439395.4	
							662.869	
DeKalb	3885.51294	4681.77	796.25706		-		634025.3	
							796.257	
Cherokee	3992.28027	4590.59	598.30973		-598.31		357974.5	

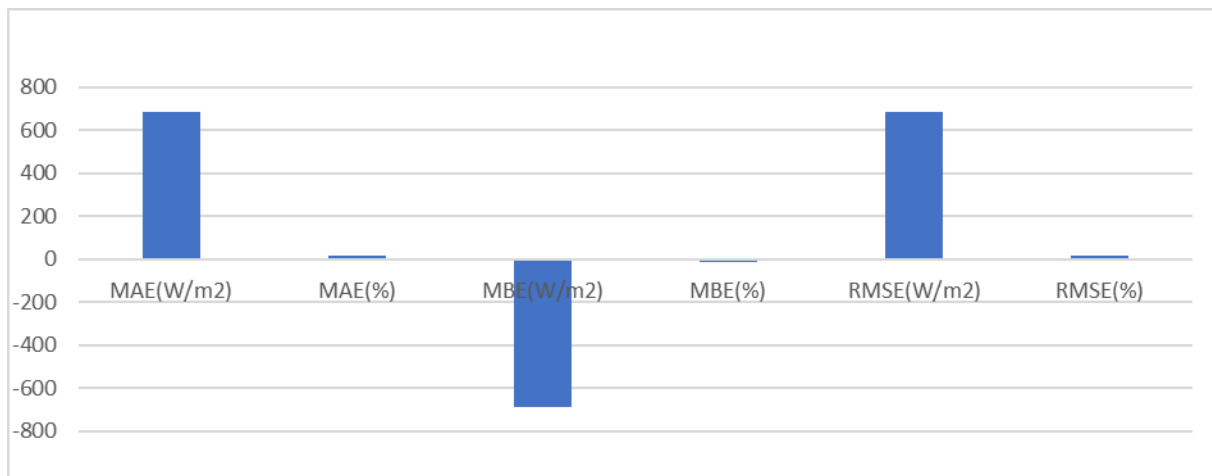


Figure 5 Results of the statistical parameters of MBE and RMSE used in the validation of calculated GHI compared against ground station measured value from the NREL network

4.3 Resulting Comparison Matrix and Weights of Physical Factors

Table 4 shows the resulting comparison matrix and the accompanying weights derived from the qualitative comparison of the identified physical factors that affect the siting of solar panels. The results revealed the factors of sunshine duration and GHI as the two factors that significantly influence the siting of panels. Both factors are of equal importance and had a weight of 38.6 % each. Aspect and slope, like the two factors mentioned earlier, were equally weighted at a value of 9.3%. Lastly, the temperature had a negligible weight value of 4.2%.

The consistency ratio gauges the measure of the resultant weights assigned to the factors. If the consistency ratio (CR) value is smaller or equal to 10%, the inconsistency is acceptable. If the consistency ratio is greater than 10 %, then the subjective judgment needs to be revised. The consistency ratio of the implemented Analytical Hierarchy Process (AHP) yielded a value of 3.29 %. The CR value is far below 10 %; hence, this affirms the accuracy of the subjective evaluation of weights that were assigned to the factors.

Table 5 Weights of various favorable criteria indicators.

	GHI	Sunshine	Slope	Aspect	Temperature	Weight	CR
GHI	1	1	5	5	7	38.6	3.294055
Sunshine	1	1	5	5	7	38.6	
Slope	0.2	0.2	1	1	3	9.3	
Aspect	0.2	0.2	1	1	3	9.3	
Temperati	0.14	0.14	0.33	0.33	1	4.2	
	2.54	2.54	12.33	12.33	21	100	

4.4 Resulting Normalized Raster Surfaces

The normalized raster surfaces of the physical suitability factor revealed that different parts of Metropolitan Atlanta have differing levels of suitability for siting solar farms. Figures 6, 7, 8, 9, and 10 show such areas for each of the physical factors that influence the siting of solar PV systems. The normalized raster had pixel values between 0 and 1.

Areas with pixel values of 0.75 and up indicates favorable sites, and those with normalized values below 0.5 represent the least favorable sites. The normalized values for aspect (Figure 4) and slope (Figure 4) indicates much of the study area satisfies the threshold needed to mount solar panels.



Figure 6 Normalized aspect raster data indicating areas favorable for solar siting based on only the aspect criterion

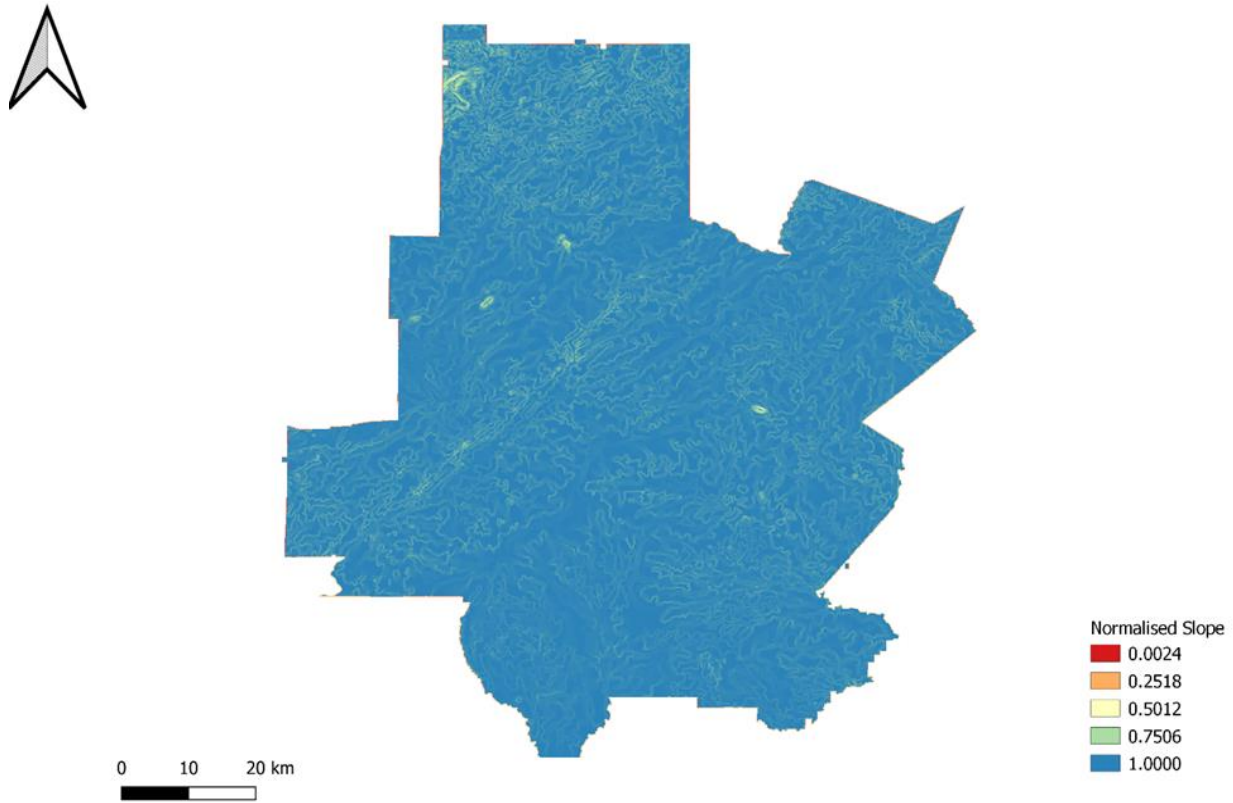


Figure 7 A normalized slope map of Metropolitan Atlanta showing suitable areas for mounting solar panels based on the slope criterion alone

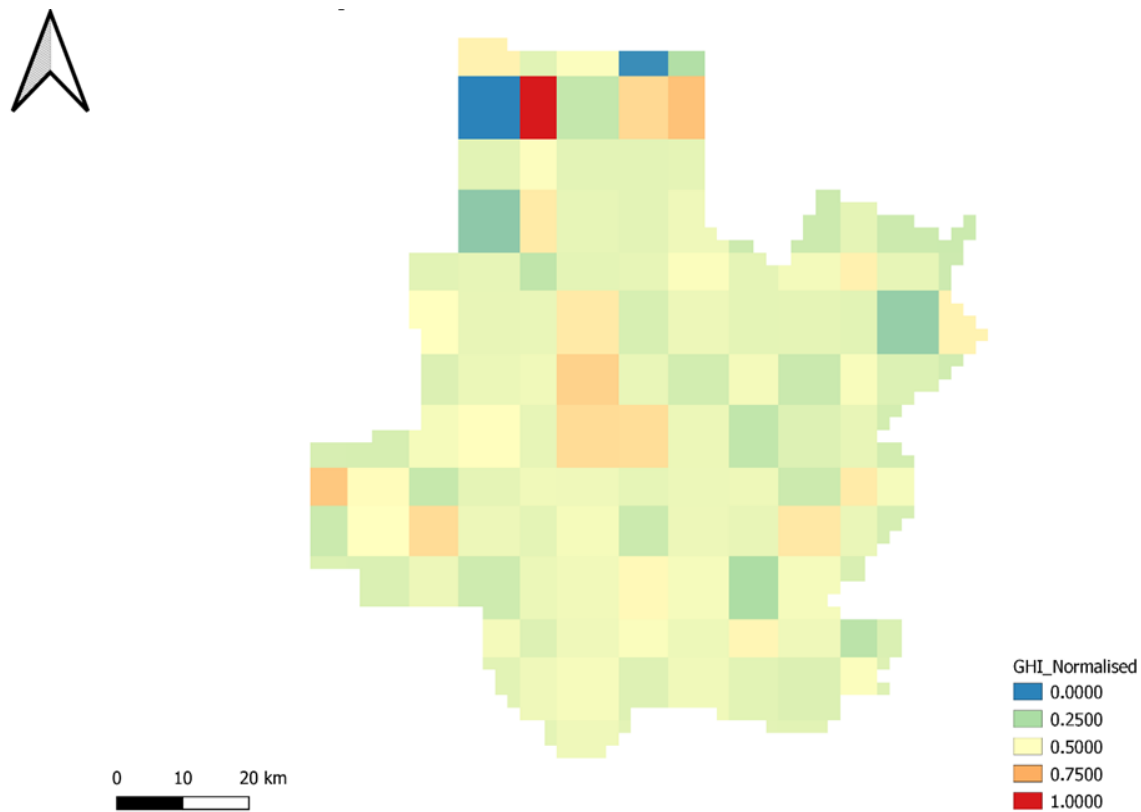


Figure 8 The map displays the normalized values of the annual GHI values of Atlanta. Blue indicates areas least favorable per the GHI criterion, while the red color shows the most area

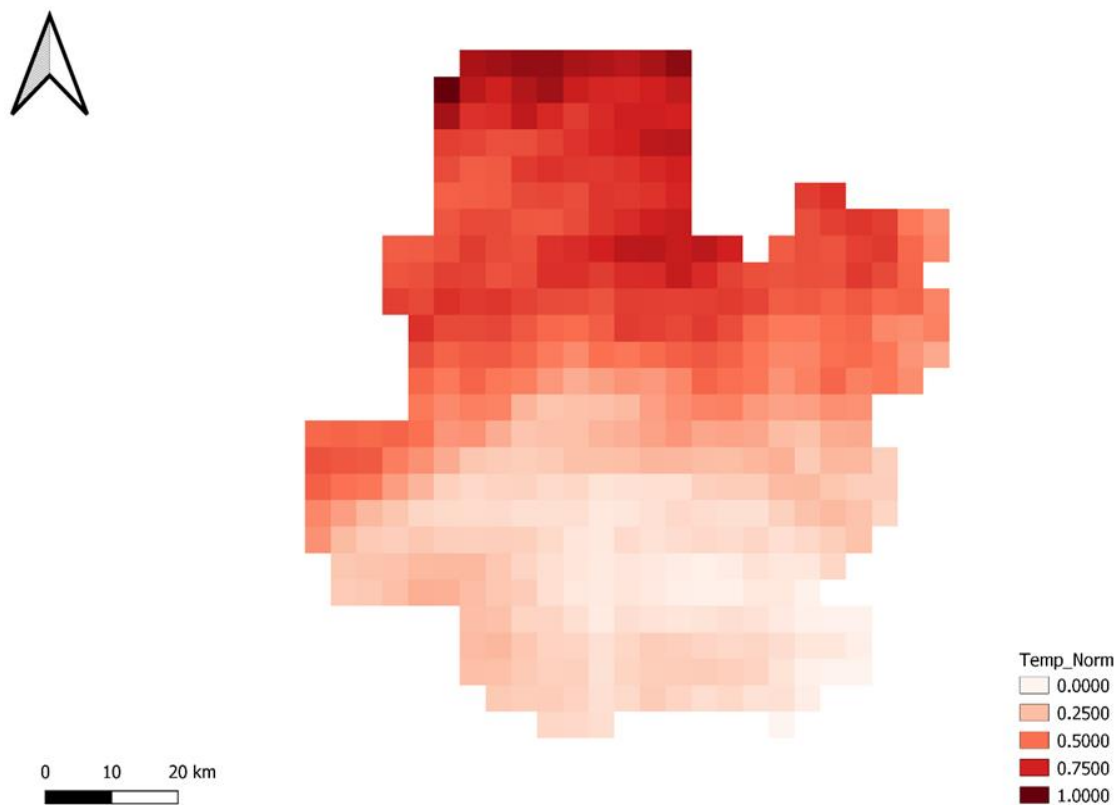


Figure 9 Normalized temperature values for Metropolitan. Areas with values of 0.75 and above are not susceptible to decreased efficiency because of temperature

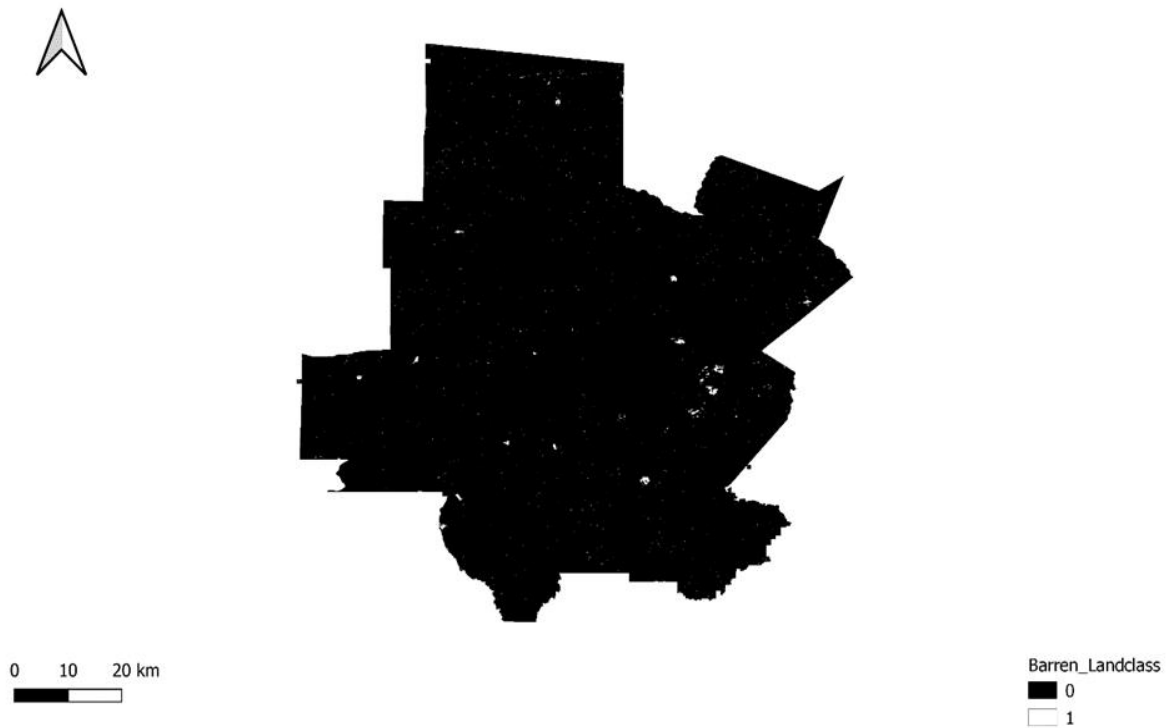


Figure 10 Normalized Map of Land Cover of Metropolitan Atlanta showing areas of bare ground designation. Developed areas unsuitable for solar siting are shown in the black coloration, while suitable areas are shown via the white coloration

4.5 Solar Composite Index

Most suitable sites with suitability index values greater than 0.7 were selected, and therefore areas suitable for siting solar PV systems in Metropolitan Atlanta were delineated (Fig. 10). More suitable sites for siting solar PV systems were in western and middle southern parts of Metropolitan Atlanta, covering a total area of 234.96 sq km, representing about 3% of the Metropolitan Atlanta territory. Also, the major proportion of the most suitable areas (80.2%) is in Dekalb, Rockdale, and Henry County, while the remaining locations were found in Fulton and Douglas County, respectively.

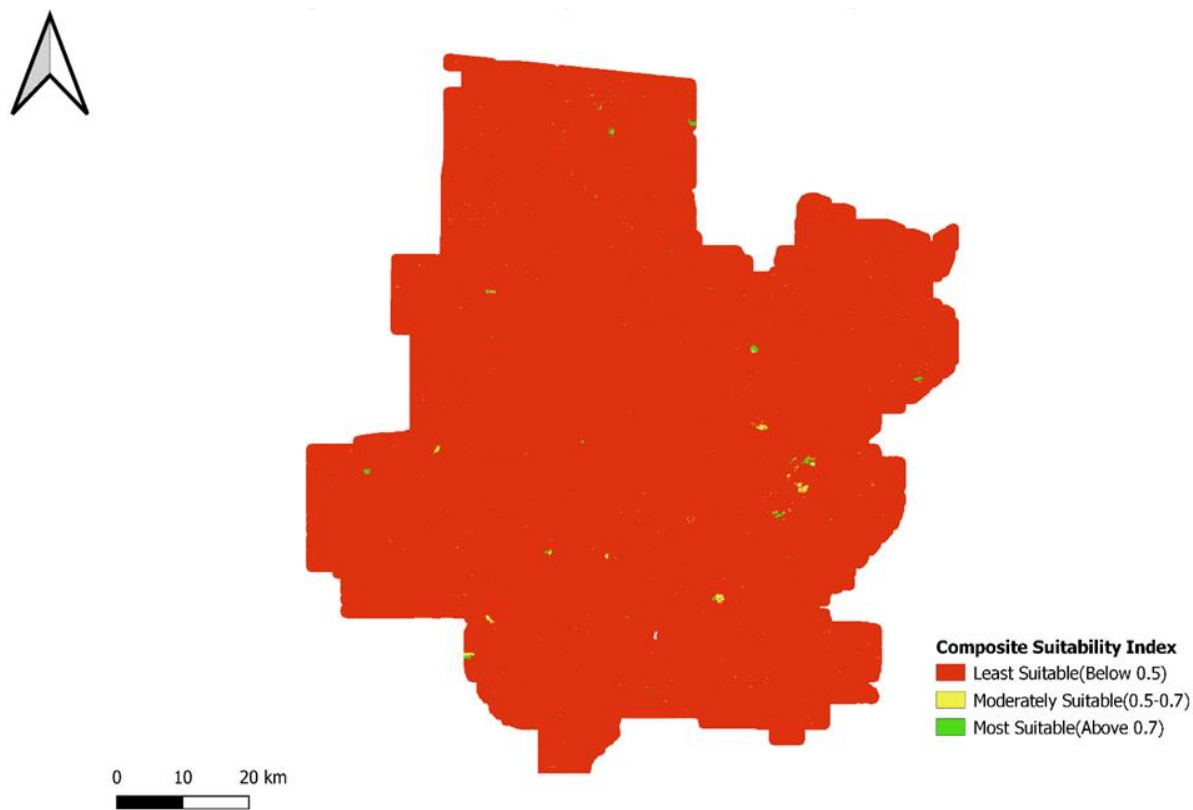


Figure 11 A map showing the solar composite suitability index for Metropolitan Atlanta.

5 DISCUSSION

The findings from this study based on Heliosat-2 calculation for Metropolitan Atlanta, located in the northern hemisphere, show the months of May, June, and July to have the highest GHI values (Figure 3), which affirms the pattern identified in past studies (e.g., Pagola et al., 2014; Vignola et al., 2007). Both Pagola et al. (2014) and Vignola et al. (2007) not only showed the summer to have the highest GHI, but they also revealed that the months of maximum GHI vary depending on geographic location and the hemisphere of the area under observation. Fillol et al.'s (2017) study in Guiana determined the months of December, January, and February as having the maximum recorded GHI values. Findings from this study somewhat deviate from previous studies in the northern hemisphere, which have shown the months of June, July, and August as the period of maximum GHI.

However, the months of maximum GHI values derived from the methodology deviate slightly from those based on ground data and research studies in similar geographic locations. Typically, ground stations observe maximum GHI values beginning the month of June through July to the end of August. Peak GHI values are reached in August, after which GHI values start to decrease. In our study, high GHI values started in May rather than June. This deviation from the established pattern could be due to the large value of the clearness index recorded for May (0.60) when compared to June (0.57), July (0.57), and August (0.56). Our findings show that May had the highest clearness index for Metropolitan Atlanta in 2019. Although maximum GHI values are typically associated with summer months (June, July, and August), in Metropolitan Atlanta, the intensity of summer GHI values is directly correlated to the atmosphere's transmissivity values (i.e., clearness index).

The Heliosat-2 methodology used for the study underestimated GHI values by 14% (Table 3 and Figure 5) points compared to the ground measured solar radiation. This finding corroborates the established conclusions of past comparisons of Heliosat-2 derived values to that of ground stations. On average, satellite-based algorithms underestimate GHI compared to observed ground-measured solar values. The range of underestimation by satellite-based algorithms falls between the 7% to 22% range observed by Marchand (2018). The RMSE of 14.84 % for the methodology adopted for the study thus falls within the acceptable range of established error.

The AHP (Table 4) found the two variables of GHI and sunshine duration as the two most consequential physical variables out of the five identified. Both had an individual weight assignment of 0.386 and cumulatively had an impact of 77.2%. This observation proves to be accurate as solar farms cannot be built without GHI, and sunshine duration is inherently coupled to GHI(Figure 12). Suehrcke, 2013 and Mujabar, 2021 studies (Figure 12) found a positive correlation between sunshine duration and GHI. A decrease in sunshine duration yields low GHI values. Thus, the output of solar power plants decreases precipitously during the season of winter. Daylight hours are shorter than 12 hours during winter, and the opposite is true during summer.

AHP also found the physical factors of slope and aspect to be a limiting factor (Yousef et al., 2018). Hence, both were assigned a weight of 0.093 each. Temperature negatively affected the efficacy of photovoltaic cells and was awarded the least weight of 0.042 out of the five physical suitability factors that were considered.

A minimum threshold of 3.5 Kw/h (Gasparovic, 2019) has been shown as the least amount of annual impinging GHI values required to establish a commercial solar farm. From figure 4, the annual average GHI values indicate Metropolitan Atlanta can support solar farms as the least

GHI value estimated was 3.7 Kw/h. The most optimal sites based on the normalized GHI (Figure 9) revealed the northern and middle portions of Metropolitan Atlanta to be the most conducive places to harness an intense amount of solar energy as the incident GHI is intense. A deviation was the pixel with the lowest GHI value and the pixel with the highest GHI value adjacent to each other. This phenomenon can be attributed to either the clearness index value or the Linke turbidity value. Both pixels had a clearness index of 0.57 but a differing value of Linke turbidity of 2.8 and 4.6, respectively. Since the clearness values are the same, the variation in GHI is not due to the clearness index/cloud coverage but rather due to the Linke Turbidity. However, no anthropogenic activity was found within the geographic span of the pixels to account for such vast variation in the Linke Turbidity. Hence, the conclusion is an error in the Linke turbidity data set values for the two pixels.

The characteristics of the aspect and the slope of the area under consideration significantly impact the intensity of solar radiation impinging on the area. Slope and aspect are considered limiting factors (Yousef et al., 2018). Suh, 2016 demonstrated the constraining designation of the slope when his study determined alternating the slope threshold between the percentages of 5 to 10 while other physical variable was held constant greatly diminished the size of suitable areas for solar farms. For a 5% threshold, only 5.1 % of the study area could support a solar, while the area of suitability increased to 9% when the threshold was pegged at 10%. Observed patterns based on past studies (Fillol et al. 2017; Gasparovic, 2019; Yousef et al., 2018) show areas of southern orientation coupled with a slope percentage below 10% received more solar radiation than locations oriented north with a slope percentage above 10%. The findings from this study found the vast majority of Metropolitan Atlanta satisfies the aspect and slope criteria. 52% of Metropolitan Atlanta (Figure 6) is south facing, while 85% (Figure 7) has a sloping incline below

10%. On the criteria of slope and aspect alone, the majority of Metropolitan Atlanta satisfies the requirement needed to host solar farms.

Hofierka J, Suri M (2002)'s study found a proportionate increase in incident GHI with increasing air temperature (Figure 13). Similarly, in Mujabar (2021)'s study of the relationship between temperature and GHI in Saudi Arabia, he concluded a positive correlation exists between GHI and temperature, thus concluding areas of high temperature will have GHI values as well. However, (Dubey 2013) study found warmer temperatures reduce photovoltaics' cells energy production. For every degree above 77 F, the solar panel experiences a drop in efficiency by 5% (Dubey,2013). The results of the normalized temperature profile for Metropolitan Atlanta show sites in the southern part of Metropolitan Atlanta (Figure 10) to be the most susceptible to decreased panel efficiency as they experience annual average temperatures above 77 F. 65% of the Metropolitan Atlanta experiences annual temperature values above the threshold of 77 F; thus, a sited solar farm is likely to experience a decrease in efficiency. Hence, the most favorable location for siting a solar farm, based on temperature, is the northern part of Metropolitan Atlanta.

Despite the influences of the physical variables considered and discussed above, the location of the delineated optimal solar sites in this study is heavily influenced by the geographic location of the bare grounds (Figure 11) identified from the land cover dataset. Ultimately, the most relevant variable that influences the optimal site selection is the availability of barren lands to accommodate the solar plant. Metropolitan Atlanta's total area of bare ground based on the landcover dataset was 234.96 sq km (Figure 10). Similarly, the size of the area identified to be optimal solar farms was equal to 234.96 sq km (Figure 11).

6 CONCLUSION

The goal of this research was in two-folds. The first goal was the assessment of the accuracy of solar data for Metropolitan Atlanta derived from Heliosat-2. Heliosat-2 methodology was used to calculate GHI values for Atlanta. The ground measured solar radiation data for stations within the NREL network of Atlanta was downloaded. The calculated GHI values were compared to ground measured radiation values using the statistical parameters MBE and RMSE. GHI values derived from the Heliosat-2 methodology had an MBE of 684.113 W/m² and an RMSE of 14.84027 %. GHI values from the Heliosat-2 method underestimated ground measured values by 14.84 %.

The second goal of this research was to delineate the suitable areas in Metropolitan Atlanta that could host solar power systems using physical suitability factors and the Analytical Hierarchy Process. GHI and other important physical parameters, including slope, aspect, temperature, land cover classes and sunshine duration hours, were applied in this research study. AHP defined the weights for each criterion or physical parameter. GHI and sunshine duration had the largest impact on solar siting, followed by slope and aspect, with temperature having the least effect on the weight obtained via AHP. Metropolitan Atlanta had a total area of 234.96 sq km viable for the installation of solar power systems.

7 RECOMMENDATION AND FUTURE WORK

For future works, the following factors need to be considered in selecting suitable sites for solar panels:

- Rooftops of buildings within Metropolitan Atlanta needs to be factored into the available space under consideration for mounting solar panels as the results of this study has a relatively small area for building solar farms.
- Information regarding the zoning designation of identified bare areas should be included in deciding which areas are suitable to exclude private lands.
- Cost criteria such as proximity to transmission lines and highways should be included in the future analysis of optimal site delineation.

REFERENCES

- A.J. Jarvis, D.T. Leedal, C.N. Hewitt. Climate-society feedbacks and the avoidance of dangerous climate change. *Nat Clim Change*, 2 (2012), pp. 668-671
- Adeh, E.H., Good, S.P., Calaf, M. et al. Solar PV Power Potential is Greatest Over Croplands. *Sci Rep* 9, 11442 (2019). <https://doi.org/10.1038/s41598-019-47803-3>
- Atsumu Ohmura et al. (1998). Baseline Surface Radiation Network (BSRN/WCRP): New Precision Radiometry for Climate Research. *Bulletin of the American Meteorological Society*, 79(10).
- Atlanta, C. o. (n.d.). *Atlanta Department of City Planning GIS*. Retrieved 06 06, 2020, from Atlanta Department of City Planning GIS: <https://gis.atlantaga.gov/>
- Beyer, H. G. (1996). Modifications of the Heliosat procedure for irradiance estimates from satellite data. *Solar Energy*, 56, 121– 207. doi:10.1016/0038-092X(95)00092-6
- Bhartia, P.K., McPeters, R.D., Mateer, C.L., Flynn, L.E., Wellemeyer, C. (1996). Algorithm for the estimation of vertical ozone profiles from the backscattered ultraviolet technique. *Journal of Geophysical Research Atmospheres*, 101(13), 18793-18806.
- C. Rigollier, M. L. (2004). The method Heliosat-2 for deriving shortwave solar radiation from satellite images. *Solar Energy*, 77, 159-169. doi:hal-00361364
- Chaoshun Liu, Y. L. (2011). Retrieval of columnar water vapor using multispectral radiometer measurements over northern China. *Journal of Applied Remote Sensing*, 5(1), 3558. doi:10.1117/1.3647483
- Christelle Rigollier, M. L. (2004). The Method Heliosat-2 For Deriving Shortwave Solar. *Solar Energy*, 2, 159-169. doi: hal-00361364

Christian A. Gueymard, D. R. (2009). Evaluation of conventional and high-performance routinesolar radiation measurements for improved solarresource, climatological trends, and radiative modeling. *Solar Energy*, 83, 171–185. doi:10.1016/j.solener.2008.07.015

Chuck Long, J. M.-L. (2014). The Baseline Surface Radiation Network: Surface Radiation Observations for Climate Research. *Global Monitoring Annual Conference* (p. 20). Bologna: World Climate Research Programme.

Claudia Emde, R. B.-S. (2016). The libRadtran software package for radiative transfer calculations. *Geoscientific Model Development*, 9, 1647–1672. doi:10.5194/gmd-9-1647-2016, 2016

D.Cano, J. M. (1986). A method for the determination of the global solar radiation from meteorological satellite data. *Solar Energy*, 37(1), 31-39. doi:10.1016/0038-092X(86)90104-0

Dumortier, D. (1995). Modelling global and diffuse horizontal irradiances under cloudless skies with different. *Daylight II, final report vol. 2. Tech. rep.*, jou2-ct92-0144.

Erwann Fillol, Tommy Albarelo, Antoine Primerose, Lucien Wald, Laurent Linguet. Spatiotemporal indicators of solar energy potential in the Guiana Shield using GOES images. *Renewable Energy*, Elsevier, 2017, 111, pp.11-25. 10.1016/j.renene.2017.03.081. hal-01512562

Atsumu Ohmura et al. (1998). Baseline Surface Radiation Network (BSRN/WCRP): New Precision Radiometry for Climate Research. *Bulletin of the American Meteorological Society*, 79(10).

Atlanta, C. o. (n.d.). *Atlanta Department of City Planning GIS*. Retrieved 06 06, 2020, from Atlanta Department of City Planning GIS: <https://gis.atlantaga.gov/>

Badescu, V.; Gueymard, C.A.; Cheval, S.; Oprea, C.; Baciu, M.; Dumitrescu, A.; Iacobescu, F.; Milos, I.; Rada, C. Accuracy analysis for fifty-four clear-sky solar radiation

models using routine hourly global irradiance measurements in Romania. *Renew. Energy* 2013, 55, 85–103

Beyer, H. G. (1996). Modifications of the Heliosat procedure for irradiance estimates from satellite data. *Solar Energy*, 56, 121– 207. doi:10.1016/0038-092X(95)00092-6

Bhartia, P.K., McPeters, R.D., Mateer, C.L., Flynn, L.E., Wellemeyer, C. (1996). Algorithm for the estimation of vertical ozone profiles from the backscattered ultraviolet technique. *Journal of Geophysical Research Atmospheres*, 101(13), 18793-18806.

C. Rigollier, M. L. (2004). The method Heliosat-2 for deriving shortwave solar radiation from satellite images. *Solar Energy*, 77, 159-169. doi:hal-00361364

Chaoshun Liu, Y. L. (2011). Retrieval of columnar water vapor using multispectral radiometer measurements over northern China. *Journal of Applied Remote Sensing*, 5(1), 3558. doi:10.1117/1.3647483

Christelle Rigollier, M. L. (2004). The Method Heliosat-2 For Deriving Shortwave Solar. *Solar Energy*, 2, 159-169. doi: hal-00361364

Christian A. Gueymard, D. R. (2009). Evaluation of conventional and high-performance routinesolar radiation measurements for improved solarresource, climatological trends, and radiative modeling. *Solar Energy*, 83, 171–185. doi:10.1016/j.solener.2008.07.015

Chuck Long, J. M.-L. (2014). The Baseline Surface Radiation Network: Surface Radiation Observations for Climate Research. *Global Monitoring Annual Conference* (p. 20). Bologna: World Climate Research Programme.

Claudia Emde, R. B.-S. (2016). The libRadtran software package for radiative transfer calculations. *Geoscientific Model Development*, 9, 1647–1672. doi:10.5194/gmd-9-1647-2016, 2016

D.Cano, J. M. (1986). A method for the determination of the global solar radiation from meteorological satellite data. *Solar Energy*, 37(1), 31-39. doi:10.1016/0038-092X(86)90104-0

Dumortier, D. (1995). Modelling global and diffuse horizontal irradiances under cloudless skies with different. *Daylight II, final report vol. 2. Tech. rep*, jou2-ct92-0144.

Engerer, N.A.; Mills, F.P. Validating nine clear sky radiation models in Australia. *Solar Energy* 2015, 120, 9–24

Erwann Fillol, Tommy Albarelo, Antoine Primerose, Lucien Wald, Laurent Linguet. Spatiotemporal indicators of solar energy potential in the Guiana Shield using GOES images. *Renewable Energy*, Elsevier, 2017, 111, pp.11-25. 10.1016/j.renene.2017.03.081. hal-01512562

Gasparovic, I. G. (2019). Determining Optimal Solar Power Plant Locations Based on Remote Sensing and GIS Methods: A Case Study from Croatia. *Remote Sensing*, 11, 1481. doi:10.3390/rs11121481

Gašparovic, I. G. (2019). Determining Optimal Solar Power Plant Locations Based on Remote Sensing and GIS Methods: A Case Study from Croatia. *Remote Sensing*(11), 1481. doi:10.3390/rs11121481

Geuder, N. et al., 2006. (2006). Examination of different irradiation sensors: operation experiences and comparative study. *4th International Conference on Experiences with Automatic Weather Stations*, (p. Solar Energy). Lisbon, Portugal.

Guanghai Huang, Z. L. (2020). Estimating surface solar irradiance from satellites: Past, present, and future perspectives. *Remote Sensing of the Environment*, 233, 111371. doi:10.1016/j.rse.2019.111371

Guanghai Huang, Z. L. (2020). Estimating surface solar irradiance from satellites: Past, present, and future perspectives. *Remote Sensing of the Environment*, 233, 111371.

doi:doi:10.1016/j.rse.2019.111371

H.Piazena. (1996). The Effect of Altitude Upon The Solar UV-B and UV-A Irradiance In The Tropical Chilean Andes. *Solar Energy*, 57(2), 133-140. doi:10.1016/S0038-092X(96)00049-

7

Hailei Liu, S. T. (2017). An improved physical split-window algorithm for precipitable water vapor retrieval exploiting the water vapor channel observations. *Remote Sensing of the Environment*, 174, Pages 366-378. doi:10.1016/j.rse.2017.03.031

Hamed Hafeznia, Hossein Yousefi, Fatemeh Razi Astaraei, A novel framework for the potential assessment of utility-scale photovoltaic solar energy, application to eastern Iran,

Energy Conversion and Management, 151, Pages 240-258,

doi.org/10.1016/j.enconman.2017.08.076.

Hofierka J, Suri M (2002) The solar radiation model for Open source GIS: implementation and applications. In: International GRASS users conference in Trento, Italy, September 2002, pp 11–13

Hossein Yousefi , Hamed Hafeznia and Amin Yousefi-Sahzabi (2018). Spatial Site Selection for Solar Power Plants Using a GIS-Based Boolean-Fuzzy Logic Model: A Case Study of Markazi Province, Iran. *Energies* 2018, 11, 1648; doi:10.3390/en11071648

I. M. Peters, S. K. (n.d.). *Urban Haze and Photovoltaics*.

Ibrahim Reda, Tom Stoffel, Daryl Myers. (2003). A method to calibrate a solar pyranometer for measuring reference diffuse irradiance. *Solar Energy*, 74(2), 103-112. doi:10.1016/S0038-092X(03)00124-5

J. Alonso-Montesinos, F.J. Batlles, J.L. Bosch, J. Alonso-Montesinos, F.J. Batlles, J.L. Bosch(2015). Beam, diffuse and global solar irradiance estimation with satellite imagery, *Energy Conversion and Management*, 105, Pages 1205-1212, doi.org/10.1016/j.enconman.2015.08.037.

J. Poloa, F. Antonanzas-Torres, J.M. Vindela, L. Ramirez. (2014). Sensitivity of satellite-based methods for deriving solar radiation to different choice of aerosol input and models. *Renewable Energy*, 68, 785-792. doi:10.1016/j.renene.2014.03.022

Jay R.S. Doorgaa, S. D. (2019). Multi-criteria GIS-based modelling technique for identifying potential solar farm sites: A case study in Mauritius. *Renewable Energy*, 133, 1201-1219. doi:10.1016/j.renene.2018.08.105

Kasten, F. (1996). THE Linke Turbidity Factor Based on Improved Values of the Integral Rayleigh Optical Thickness. *Solar Energy*, 56(3), 239-244. doi:0038-092X(95)00114-X

Khemiri, W., Yaagoubi, R., Miky, Y., 2018. Optimal Placement of Solar Photovoltaic Farms Using Analytical Hierarchical Process and Geographic Information System in Mekkah, Saudi Arabia. in: 1st International Congress on Solar Energy Research, Technology and Applications (ICSERTA 2018), May 8-10 2018 Ouarzazate, Morocco AIP, 020025-1–020025-10 10.1063/1.5084998

Laszlo, P. a. (1992). Modeling surface solar irradiance for satellite applications on a global scale. *Journal of Applied Meteorology*, 31, 194-211.

M. Hess, P. K. (1998). Optical properties of aerosol and clouds: the software package OPAC. *Bulletin of the American Meteorological Society*, 79, 831-844. doi:10.1175/1520-0477(1998)079<0831:OPOAAC>2.0.CO;2

M.A. Hassaan, A. Hassan and H. Al-Dashti, GIS-based suitability analysis for siting solar power plants in Kuwait, *The Egyptian Journal of Remote Sensing and Space Sciences*, <https://doi.org/10.1016/j.ejrs.2020.11.004>

Mujabar, S., Chintaginjala Venkateswara, R. Empirical models for estimating the global solar radiation of Jubail Industrial City, the Kingdom of Saudi Arabia. *SN Appl. Sci.* 3, 95 (2021). <https://doi.org/10.1007/s42452-020-04043-9>

Mayer, B. a. (2020). The libRadtran software package for radiative transfer calculations - description and examples of use. *Atmospheric Chemistry and Physics*, 20, 3317–3332. doi:10.5194/acp-20-3317-2020, 2020

Michel Journée, C. (2010). Improving the spatio-temporal distribution of surface solar radiation data by merging ground and satellite measurements. *Remote Sensing of Environment*, 114(11), 2692-2704. doi:10.1016/j.rse.2010.06.010

Myers, D.R. et al. (2002). Recent progress in reducing the uncertainty in and improving pyranometer calibration. *Solar Energy Engineering, Transactions of the ASME*, 124, 44–50. doi:10.1115/1.1434262

NREL. (2021, November 10). *NREL Research*. Retrieved from NREL: www.nrel.gov

Page, J. (1996). Algorithms for the Satellight programme. *Projektinterner Bericht Tech rep.*

Rasool, S. (1964). Global distribution of net energy balance of atmosphere from Tiros radiation data. *Science*, *143*, 567.

Resilience, C. o. (2017, May 15). *Clean Energy Atlanta*. Retrieved April 29, 2020, from 100atl: www.100atl.com

Richard Perez, R. A. (1997). Comparing satellite remote sensing and ground network measurements for the production of site/time specific irradiance data. *Solar Energy*, *60*(2), 89-96. doi:10.1016/S0038-092X(96)00162-4

Robert E. Holz, S. P. (2016). Resolving ice cloud optical thickness biases between CALIOP and MODIS using infrared retrievals. *Atmospheric Physics and Chemistry*, *16*, 5075–5090. doi:10.5194/acp-16-5075-2016, 2016

Schmetz, J. P. (2002). An introduction to Meteosat Second Generation (MSG). *Bulletin of the American Meteorological Society*, *83*, 977-992.

Schneider SH Easterling WE Mearns LO. 2000. Adaptation: Sensitivity to natural variability, agent assumptions, and dynamic climatic changes. Climatic Change. 45: 203-221

Swapnil Dubey, Jatin Narotam Sarvaiya, Bharath Seshadri(2013).Temperature Dependent Photovoltaic (PV) Efficiency and Its Effect on PV Production in the World – A Review,*Energy Procedia*, *33*, Pages 311-321, <https://doi.org/10.1016/j.egypro.2013.05.072>.

Uyan, Mevlut, 2013. GIS-based solar farms site selection using analytic hierarchy process (AHP) in Karapinar region, Konya/Turkey. *Renew. Sustain. Energy Rev.* *28*, 11–17. <https://doi.org/10.1016/j.rser.2013.07.042>.

Vignola F., Harlan P., Perez R., Kmiecik M. Analysis of satellite derived beam and global solar radiation data, *Solar Energy*, Volume 81, Issue 6, June 2007, Pages 768-772, ISSN 0038-092X, 10.1016/j.solener.2006.10.003

Whitaker, Rozann, 2007. Validation examples of the analytic hierarchy process and analytic network process. *Math. Comput. Modell.* 46, 840–859. <https://doi.org/10.1016/j.mcm.2007.03.018>.

Whitlock, C. H. (1995). First global WCRP shortwave surface radiation budget dataset. *Bulletin of American Society of Meteorology*, 76, 905-922.

Y.C. Zhang, W. R. (2004). Calculation of radiative fluxes from the surface to top of atmosphere based on ISCCP and other global data sets: Refinements of the radiative transfer model and the input data. *Journal of Geophysical Research*, 109. doi:10.1029/2003JD004457